Lateral response of rigid monopiles subjected to cyclic loading
Centrifuge modelling

Li, Qiang; Askarinejad, Amin; Gavin, Keneth

DOI
10.1680/jgeen.20.00088

Publication date
2021

Document Version
Final published version

Published in
Proceedings of the Institution of Civil Engineers: Geotechnical Engineering

Citation (APA)
Li, Q., Askarinejad, A., & Gavin, K. (2021). Lateral response of rigid monopiles subjected to cyclic loading: Centrifuge modelling. *Proceedings of the Institution of Civil Engineers: Geotechnical Engineering*, *175*(4), 426-438. https://doi.org/10.1680/jgeen.20.00088

Cite this article
Li Q, Askarinejad A and Gavin K
Lateral response of rigid monopiles subjected to cyclic loading: centrifuge modelling.
Proceedings of the Institution of Civil Engineers – Geotechnical Engineering,
https://doi.org/10.1680/jgeen.20.00088

Research Article
Paper 2000088
Received 04/05/2020;
Accepted 27/07/2020

Keywords: dynamics/offshore engineering/piles & piling

Geotechnical Engineering

ice Publishing

Lateral response of rigid monopiles subjected to cyclic loading: centrifuge modelling

Qiang Li
Faculty of Civil Engineering and Geosciences, Delft University of Technology, Delft, The Netherlands

Keneth Gavin
Faculty of Civil Engineering and Geosciences, Delft University of Technology, Delft, The Netherlands

Amin Askarinejad
Faculty of Civil Engineering and Geosciences, Delft University of Technology, Delft, The Netherlands (Orcid:0000-0002-7060-2141)
(corresponding author: a.askarinejad@tudelft.nl)

In this study, a total number of 20 centrifuge tests were carried out to investigate monopile behaviour under lateral cyclic loading. The instrumented model pile simulates an offshore wind turbine foundation with an embedment ratio of 5 installed in sand layers with two relative densities of 80% and 50%. The influence of the directional characteristic and amplitude of cyclic load on pile lateral behaviour was studied. The data analysis focused on the influence of cyclic load on the accumulation of lateral displacement and evolution of secant stiffness of the foundation system. The most damaging cyclic load type (which can cause the most accumulated pile displacement) is identified as two-way loading, and it was observed that cyclic load always increases the pile secant stiffness. A new model for the prediction of evolution of accumulated displacement and change in secant stiffness has been formulated. An example of the procedure developed is presented for a typical field monopile subjected to cyclic loading. Lastly, the performance of the new model is demonstrated and predicted results are compared with field test data.

Notation

C_C	curvature coefficient of sand
C_U	uniformity coefficient of sand
D	pile outer diameter
D_{50}	average grain size of sand
D_r	relative density of sand
E	elasticity modulus
e	loading eccentricity
e_{max}	maximum void ratio of sand
e_{min}	minimum void ratio of sand
G_S	specific gravity of sand
H	lateral load
H_{max}	maximum load in the loading cycle
H_{min}	minimum load in the loading cycle
H_u	pile lateral capacity
I	moment of inertia
K	secant stiffness
K_1	secant stiffness in the first cycle
K_c	non-dimensional function
K_N	secant stiffness in the Nth cycle
K_S	secant stiffness in monotonic loading phase
K_s	dimensional function for pile stiffness
L	pile length
N	cycle number
R_b	non-dimensional function
R_c	non-dimensional function
T_b	non-dimensional function
T_c	non-dimensional function
t	pile wall thickness
y	lateral displacement
$y_{max,1}$	maximum pile lateral displacement in the first cycle
$y_{max,N}$	maximum pile lateral displacement in the Nth cycle
$y_{max,S}$	pile lateral displacement at the end of monotonic loading phase
α	displacement accumulation rate
β	secant stiffness accumulation rate
ζ_b	cyclic load amplitude ratio
ζ_c	cyclic load directional characteristic ratio
θ_N	accumulated pile rotation in the Nth cycle
ϕ_{cr}	critical friction angle of sand

1. Introduction

The proportion of monopiles as offshore wind turbine (OWT) foundations has increased from approximately 75% in 2012 (Doherty and Gavin, 2011) to more than 87% in 2019 (Fan *et al.*, 2019). However, current design codes are largely based on application from the oil and gas industry. The fundamental difference between monopiles used as OWT foundations and those in the oil and gas industry is the lower embedment ratio (L/D, where L is the embedment length and D is the diameter of the pile) generally used for OWT foundations, ranging between 3 and 6 (Wu *et al.*, 2019). These foundations are subjected to a large number of load cycles, and strict permanent rotational limits are imposed. Moreover, OWTs are dynamically sensitive structures and slight changes in stiffness of the foundation might result in an undesirable shift in the natural frequency of the whole structure. Therefore, understanding the influence of cyclic load on the accumulation of lateral displacement and change in the foundation stiffness is very important to the safe design of these structures.

A number of experimental studies have been conducted to investigate the response of monopiles under lateral cyclic load (Abadie *et al.*, 2018; Askarinejad *et al.*, 2017; Gerber and Rollins, 2008; Klinkvort *et al.*, 2011; Klinkvort and Hededal, 2013; LeBlanc *et al.*, 2010; Li *et al.*, 2010; Li *et al.*, 2015; Møller and Christiansen, 2011; Nicolai *et al.*, 2017; Peralta, 2010; Roesen *et al.*, 2012; Truong *et al.*, 2018; Verdure *et al.*, 2003; Yang *et al.*, 2019; Yoo *et al.*, 2013). Two non-dimensional parameters are widely used to describe the applied cyclic loads

1. $\zeta_b = \frac{H_{max}}{H_u}$

2. $\zeta_c = \frac{H_{min}}{H_{max}}$

where H_u is defined as the pile lateral capacity determined from a monotonic test; H_{min} is the minimum load in a loading cycle; and H_{max} is the maximum load in the same cycle. The value of ζ_b can be used to define the load amplitude for cyclic loading, while ζ_c can be used to describe the directional characteristic of the cyclic loading. A visual interpretation of these two parameters is given in Figure 1.

LeBlanc *et al.* (2010) carried out 1***g*** experiments on a pile with L/D ratio of 4.5 embedded in a dry, loose sand ($D_r = 4$–38%) layer. It was found that the most damaging cyclic load type (the cyclic type which can cause the most accumulated pile displacement) is two-way loading with $\zeta_c = -0.6$. Moreover, they reported that the secant stiffness increased with the number of cycles. Klinkvort *et al.* (2011) carried out a centrifuge test series simulating cyclic loads on a monopile with L/D of 6 in dense sand ($D_r = 79$–96%). It was indicated that two-way loading ($\zeta_c = -0.4$) is the most damaging load situation. However, they observed that the secant stiffness for each cycle tends to decrease at large number of cycles when $\zeta_c > 0.1$. However, based on the results of a second series of centrifuge tests using a similar pile ($L/D = 6$) and sand ($D_r = 90\%$), Klinkvort and Hededal (2013) showed that one-way loading ($\zeta_c = 0$) is the most damaging load type. Although LeBlanc *et al.* (2010) reported that accumulation of rotation was regardless of the directional characteristic of the loading; this was in contrast to the observations reported by Klinkvort and Hededal (2013), where it was seen that the pile starts to move back towards its initial position in two-way loading where $\zeta_c \leq -0.63$.

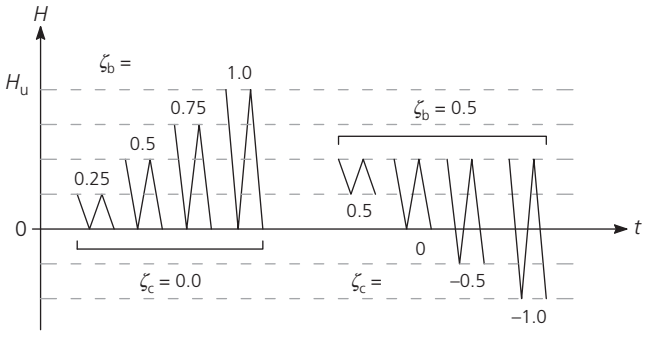

Figure 1. Characteristic of cyclic loading defined in terms of ζ_b and ζ_c

In the framework of this study, a series of centrifuge model tests has been conducted to simulate open-ended monopiles with an embedment ratio of 5 subjected to both significant lateral load and overturning moment. Given the contrasting findings from previous studies, this work focuses on two important issues for the design of monopile foundations for offshore wind turbines, namely: (*a*) the accumulation of the lateral displacement; (*b*) the evolution of the secant stiffness per loading cycle. The impacts of number of cycles, load magnitude and the directional characteristic of loading on these properties were captured by a model framework featured with both non-dimensional and dimensional functions.

2. Centrifuge model test

The tests were performed using the beam centrifuge of the Geo-Engineering Section at TU Delft, the Netherlands (Allersma, 1994; Zhang and Askarinejad, 2019a, 2019b). These tests were conducted at 100 times the gravitational acceleration (100***g***). A two-dimensional actuator (Figure 2) was used to impose lateral load (H) at the pile head. A specially designed, friction-reducing ball connection was constructed to enable the application of lateral load without inducing any rotational fixity at the pile head. The detailed information on the actuator and the friction-reducing ball connection can be found in Li *et al.* (2020).

2.1 Model pile characteristics and installation

An open-ended aluminium tubular pile was used, with an outer diameter (D) of 18 mm and a wall thickness (t) of 1 mm. The load eccentricity e and the embedment depth L of the pile were kept constant at $e = 8D$ and $L = 5D$, respectively. The primary dimensions and material properties of the pile are provided in Table 1.

The model piles were installed at 1***g*** by jacking at a constant rate. However, 1***g*** installation does not represent the prototype installing technique and might result in discrepancy in the lateral stiffness and capacity of the pile (Verdure *et al.*, 2003). Fan *et al.* (2019) has identified that the difference in initial stiffness and lateral capacity of piles installed at 1***g*** and 100***g*** is less than 10%.

2.2 Soil characteristics and specimen preparation technique

The geotechnical properties of the sand used in this series of tests are summarised in Table 2. The ratio of pile diameter to

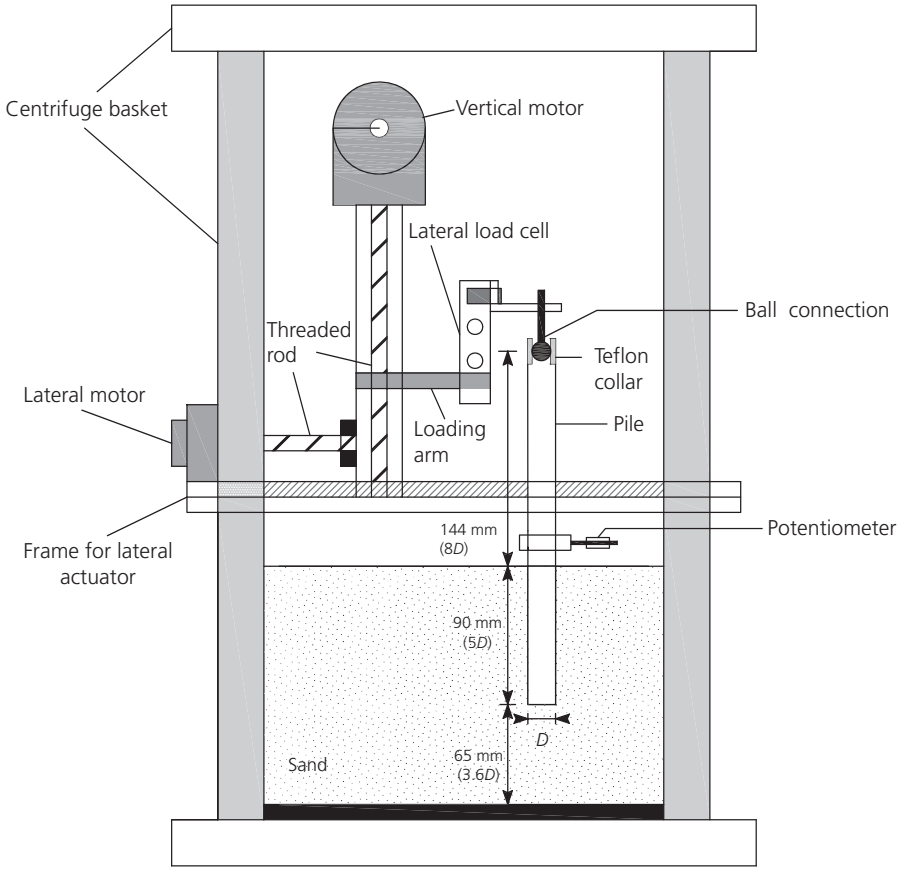

Figure 2. Schematic diagram of the two-dimensional loading actuator

Table 1. Characteristics of the model and prototype piles

Property	Model value	Prototype value[a]
Length (embedded + additional)	90 + 150 mm	9 + 15 m
External diameter	18 mm	1.8 m
Wall thickness	1 mm (aluminium)	30 mm (steel)
Young's modulus (E)	70 GPa (aluminium)	210 GPa (steel)
Stiffness (EI)	0.137 kPa m^4	13.7 GPa m^4
Load eccentricity above sand surface	144 mm	14.4 m

[a]Assume the prototype pile is made in steel
Adapted from Li *et al*. (2020)

Table 2. Basic properties of Geba sand

Property	Sand
Average grain size, D_{50}: mm	0.11
Curvature coefficient, C_C	1.24
Uniformity coefficient, C_U	1.55
Specific gravity, G_S	2.67
Maximum void ratio, e_{max}	1.07
Minimum void ratio, e_{min}	0.64
Critical friction angle, ϕ_{cr}: degrees	35

De Jager *et al*. (2017); Maghsoudloo *et al*. (2017); Maghsoudloo *et al*. (2018)

average grain size of the sands (D/D_{50}) is 164, which is larger than the values of 20 and 60 suggested by Gui *et al*. (1998) and Remaud (1999), respectively, where grain size effect becomes negligible for both vertically and laterally loaded piles (Garnier *et al*., 2007; Nunez *et al*., 1988).

Dry sand was pluviated into a rectangular model container (centrifuge strongbox) with dimensions of 400 (length) × 150 (width) × 180 (height) mm^3. Two series of homogeneous sand specimens with relative densities (D_r) of 80% and 50% were prepared.

Table 3. List of centrifuge tests

Test no.	Type	D_r: %	ζ_c	ζ_b	No. of cycles	α	β
1	Monotonic	80	—	—	—	—	—
2	Monotonic	50	—	—	—	—	—
3	Cyclic	80	−0.75	0.2	153	0.0448	0.0217
4	Cyclic	80	−0.50	0.2	143	0.0668	0.0233
5	Cyclic	80	−0.25	0.2	142	0.0674	0.0264
6	Cyclic	80	0	0.2	42	0.0581	0.0122
7	Cyclic	80	0.25	0.2	150	0.0640	0.0032
8	Cyclic	80	0.50	0.2	141	0.0610	0.0051
9	Cyclic	80	0.75	0.2	151	0.0592	0.0079
10	Cyclic	80	0	0.3	152	0.0791	0.0143
11	Cyclic	80	0	0.4	62	0.0611	0.0178
12	Cyclic	80	0	0.5	102	0.0652	0.0317
13	Cyclic	50	−0.67	0.2	61	0.0838	0.0280
14	Cyclic	50	−0.33	0.2	50	0.0888	0.0146
15	Cyclic	50	0	0.2	151	0.0878	0.0087
16	Cyclic	50	0.33	0.2	67	0.0557	0.0167
17	Cyclic	50	0.67	0.2	152	0.0549	0.0115
18	Cyclic	50	0	0.3	122	0.0816	0.0148
19	Cyclic	50	0	0.4	83	0.0840	0.0210
20	Cyclic	50	0	0.5	151	0.0708	0.0374

2.3 Loading test programme

Two monotonic and 18 cyclic tests were performed; see Table 3. The effect of load amplitude was investigated by changing ζ_b ($\zeta_b \in (0.2, 0.3, 0.4, 0.5)$) while keeping $\zeta_c = 0$, in both dense and medium dense sand layers. Several values of ζ_c with intervals of $\Delta\zeta_c = 0.25$ in dense sand ($D_r = 80\%$) and $\Delta\zeta_c = 0.33$ in medium dense sand ($D_r = 50\%$) were tested to investigate the effect of load directional characteristic on the lateral behaviour of the monopiles. The lateral load was measured at pile head.

3. Centrifuge model test results

3.1 Monotonic tests

In order to find the pile lateral capacity in dense sand and medium dense sand, respectively, two monotonic load tests were performed under a displacement-controlled condition, where the pile was loaded at a constant displacement rate of 0.02 mm/s. A test repeatability check was done and the test results are shown in Figure 3. The test data presented in this paper are in prototype scale, unless otherwise noted.

As $e = 8D$, $L = 5D$, the pile pivot point is usually assumed to be located at $0.7L$ (Chortis *et al.*, 2020; Haiderali *et al.*, 2014). Therefore, the lateral displacement at the sand surface is equal to 0.3 times the lateral displacement at the pile head. From Figure 3, the load–displacement curves did not reach a peak – that is, the maximum pile lateral resistance – in any of the tests. Therefore, a lateral reference capacity, H_u, was defined at a lateral displacement of 0.135 m ($0.075D$) at the sand surface. Therefore, the pile lateral capacities were determined to be 600 kN and 440 kN in dense and medium dense sand layers, respectively.

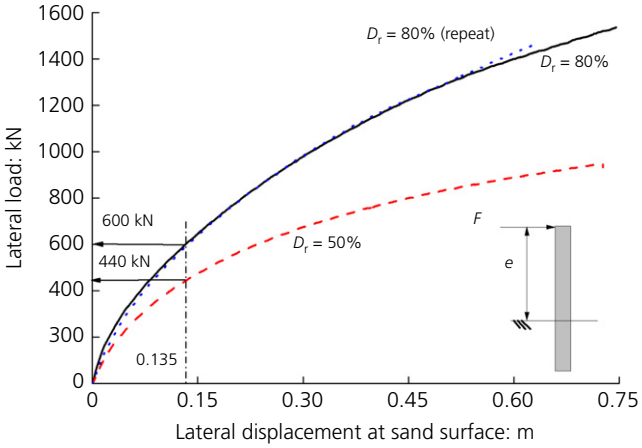

Figure 3. Monotonic test results

3.2 Cyclic tests

The range of amplitudes of cyclic loads has been selected based on the pile lateral capacity (H_u). The cyclic load tests were carried out under a load-controlled condition. Examples of the cyclic test series performed are shown in Figure 4. The first loading phase of the cyclic loads fit the monotonic loading curves quite well, which is an indication of the repeatability of the tests.

A power law (Klinkvort and Hededal, 2013; LeBlanc *et al.*, 2010) is used to relate the accumulation rate of lateral displacement to the number of load cycles

$$3. \quad \frac{y_{\max,N}}{y_{\max,S}} = N^{\alpha}$$

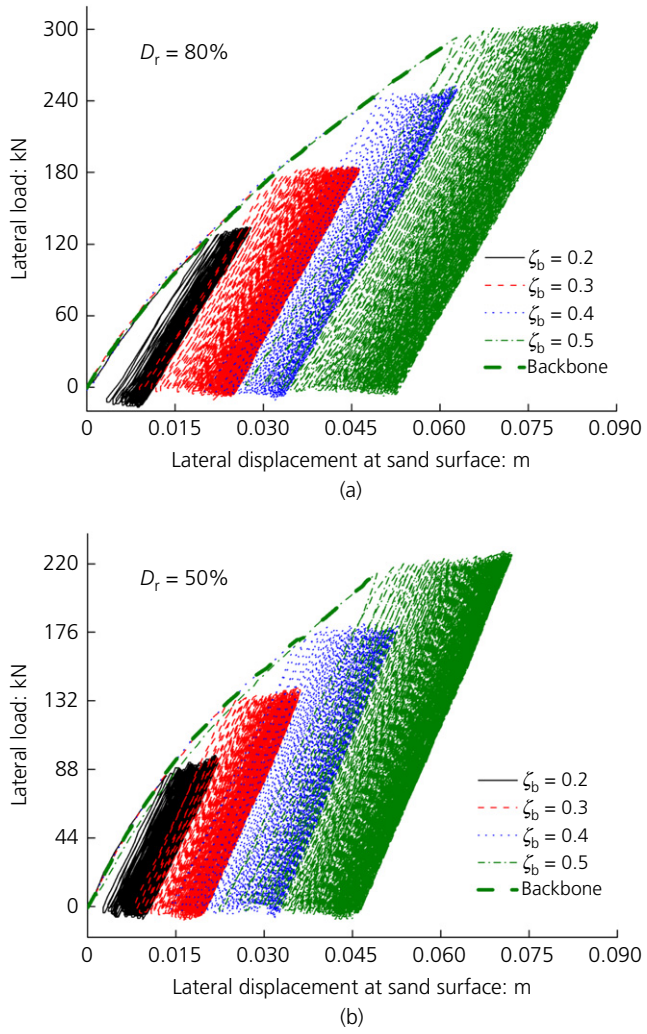

Figure 4. Pile lateral load–displacement response during cyclic load tests for the case of $\zeta_c = 0$: (a) $D_r = 80\%$; (b) $D_r = 50\%$

where $y_{max,N}$ is the lateral displacement corresponding to H_{max} at the Nth cycle and $y_{max,S}$ is the lateral displacement corresponding to H_{max} at the end of the monotonic loading phase. A schematic illustration of these two parameters is shown in Figure 5. Figure 6 shows an example of the normalised maximum lateral displacement ($y_{max,N}/y_{max,S}$) for a one-way loading test (test number 10 in Table 3). The values of α for all tests are listed in Table 3.

3.2.1 Influence of load directional characteristic ratio (ζ_c) on the accumulated lateral displacement

Twelve cyclic tests were performed in both dense and medium dense sand specimens to identify the most damaging load type in terms of accumulated lateral displacement. Parameter α from Equation 3 is used as an indication and is shown in Figure 7 as a function of ζ_c for both dense and medium dense sand specimens. In this series of tests, ζ_b is kept constant at 0.2 and the value of ζ_c is changing. According to LeBlanc *et al.* (2010) when $\zeta_c = -1$, it is expected that α would be zero, since the load applied is equal in both directions. The two dashed lines in Figure 7 are the best fits of the two series of test data.

It can be observed that the sand relative density has an influence on the value of α – that is, in general α is higher for the pile installed in the sand layer with lower relative density. This observation is more pronounced in cases of two-way loading conditions ($\zeta_c \leq 0$), and for larger values of ζ_c the effect of relative density is minor. Moreover, it can be observed that the values of α do not vary much as a function of ζ_c for medium dense sand with $D_r = 50\%$ in the range of $\zeta_c \in [-0.67, 0]$.

From the data presented, the maximum value of α was found to lie in the range between $\zeta_c = -0.25$ and -0.5. The peak value of α is not that obvious, but perhaps could be located at $\zeta_c = -0.4$. The positive value of α for all of the tests indicates

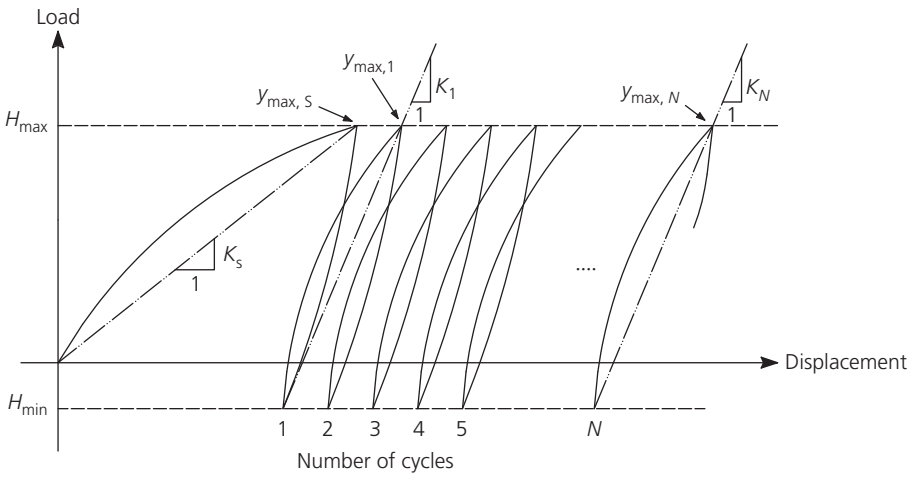

Figure 5. Schematic drawing of determination of maximum and minimum accumulated lateral displacements

that under all of the loading types the pile always accumulates displacement in one direction (the direction of the first monotonic loading). The phenomenon whereby the pile starts to move back towards its initial position in some two-way loading conditions ($\zeta_c \leq -0.63$), as reported by Klinkvort and Hededal (2013), was not observed in this research.

3.2.2 Influence of load amplitude ratio (ζ_b) on the accumulated lateral displacement

The effects of cyclic load amplitude on the accumulated pile lateral displacement regime were investigated by keeping $\zeta_c = 0$ (one-way loading) while changing ζ_b from 0.2 to 0.5. Eight cyclic tests were performed in dense and medium dense sand layers. The value of α derived from the results of these tests is plotted in Figure 8. It can be seen that α is not sensitive to the sand relative density under this specific loading case. Moreover, α is barely influenced by the load amplitude ratio ζ_b. These observations fit well with the results reported by Truong *et al.* (2018), in which the accumulation coefficient of lateral displacement was found not to be sensitive to the cyclic magnitude ratio (ζ_b), but varied with the cyclic directional characteristic ratio (ζ_c).

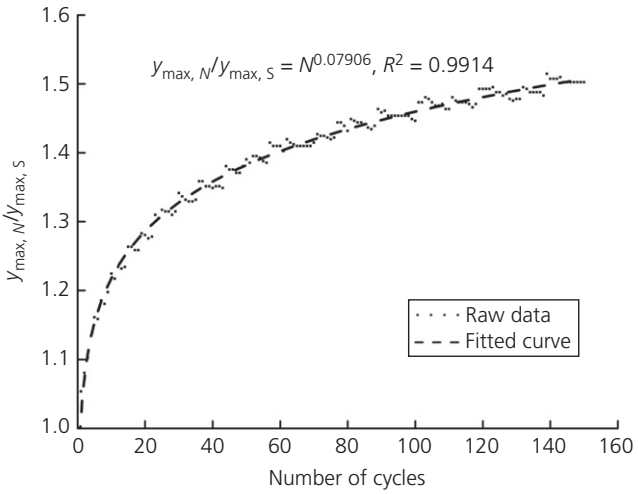

Figure 6. Normalised maximum lateral displacement from every cycle: $D_r = 80\%$, $\zeta_c = 0$, $\zeta_b = 0.3$ (test number 10 in Table 3)

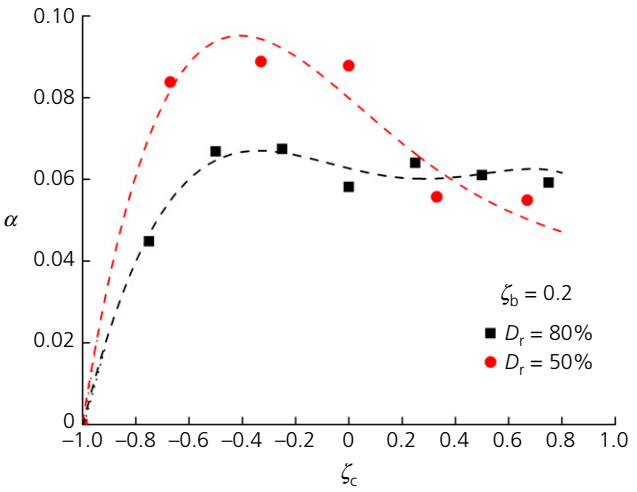

Figure 7. Load directional characteristic effects from cyclic tests

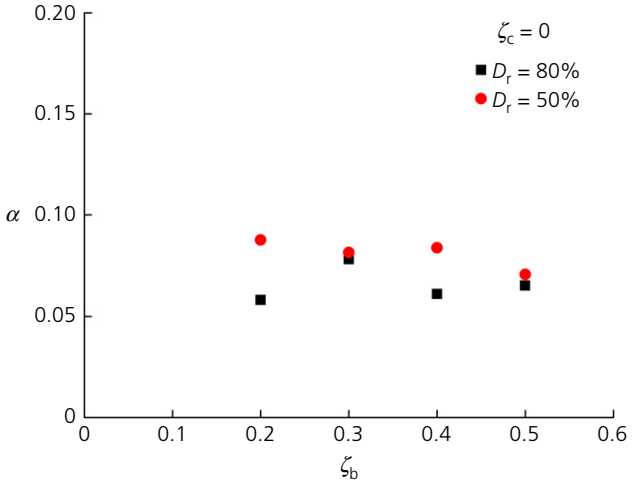

Figure 8. Load amplitude effects from cyclic tests

3.3 Effect of number of loading cycles on the pile secant stiffness

The secant stiffness (K) is defined here as the ratio between load increment and displacement increment during a loading phase (either monotonic or cyclic), as illustrated in Figure 5.

The secant stiffness in the monotonic loading phase, K_S, is calculated based on the first monotonic loading according to Equation 4

$$4. \quad K_S = \frac{H_{max}}{y_{max,S}}$$

where H_{max} is the maximum load applied in the monotonic loading phase; $y_{max,S}$ is the lateral displacement corresponding to H_{max} at the end of the monotonic loading phase.

The secant stiffness under cyclic loading, K_N (for cycle N), is calculated based on the following equation:

$$5. \quad K_N = \frac{H_{max} - H_{min}}{y_{max,N} - y_{min,N}}$$

where H_{max} and H_{min} are the maximum and minimum loads applied in the cyclic load test; and $y_{max,N}$ and $y_{min,N}$ are the

lateral displacements corresponding to H_{max} and H_{min} for cycle N, respectively.

In Figure 9, the relative secant stiffness K_N/K_1 is plotted against the number of cycles on a logarithmic scale. It is evident that secant stiffness increases with the number of cycles in all the loading cases investigated. In a similar fashion to the evolution of relative maximum lateral displacement ($y_{max,N}/y_{max,S}$), the evolution of secant stiffness can also be approximated by a power function

$$\frac{K_N}{K_1} = N^{\beta} \quad (6)$$

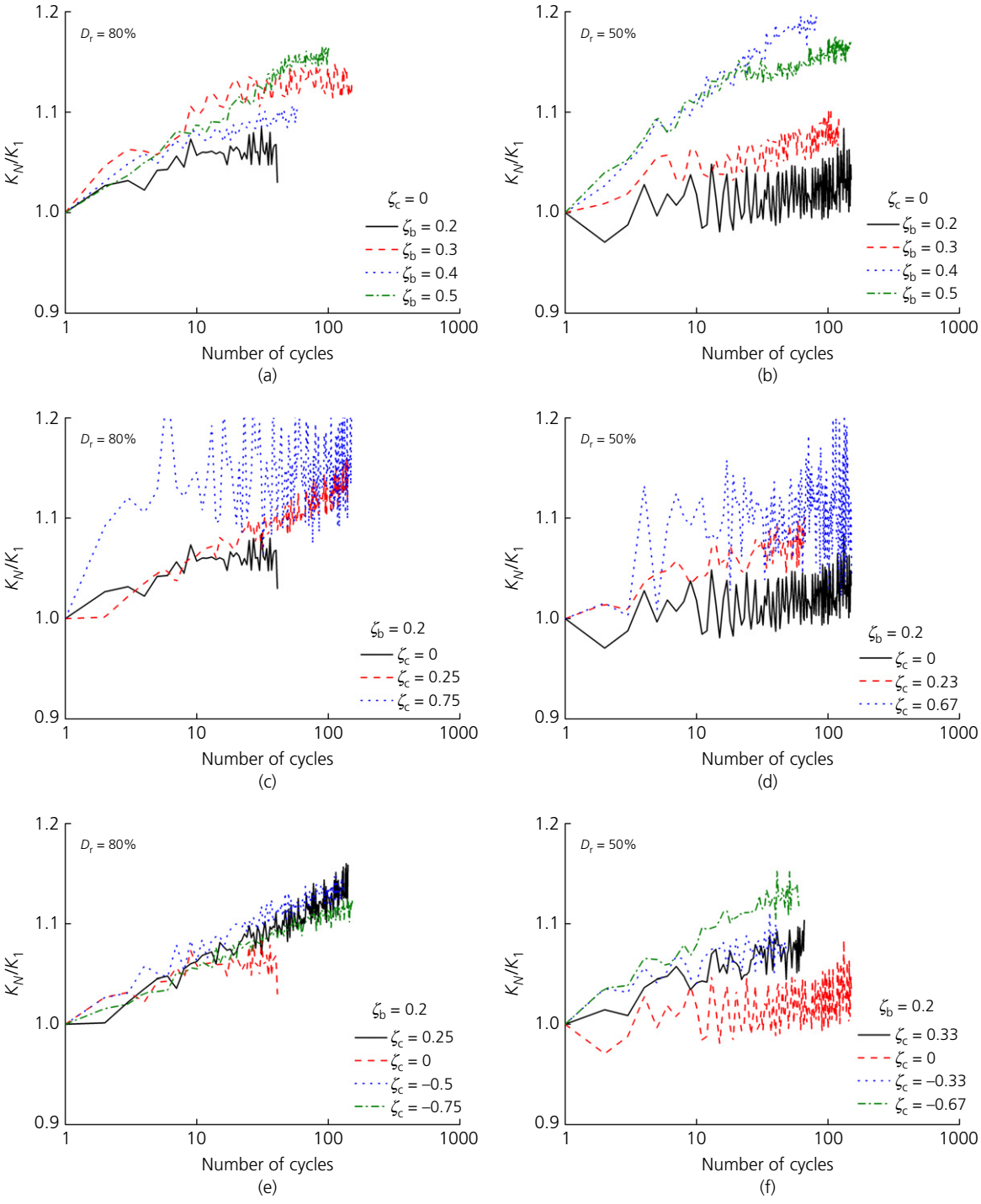

Figure 9. Change in secant stiffness from cyclic tests

The results of the fitted power function are summarised for each test in Table 3.

The values of β from Table 3 are plotted in Figures 10(a) and 10(b) as functions of ζ_c and ζ_b, respectively, in both dense sand and medium dense sand.

From Figure 10(a), a linear dependency of β on cyclic directional characteristic ratio ζ_c can be found

$$\beta = 0.015 - 0.013\zeta_c \quad (7)$$

All the β values are positive, which means the secant stiffness keeps increasing as a function of the number of cycles for all of the investigated cyclic directional characteristic ratios (ζ_c). It should also be noticed that a gradual transition from one-way to two-way loading (i.e. travelling from right to left along the x-axis of Figure 10(a)) leads to an increase of β.

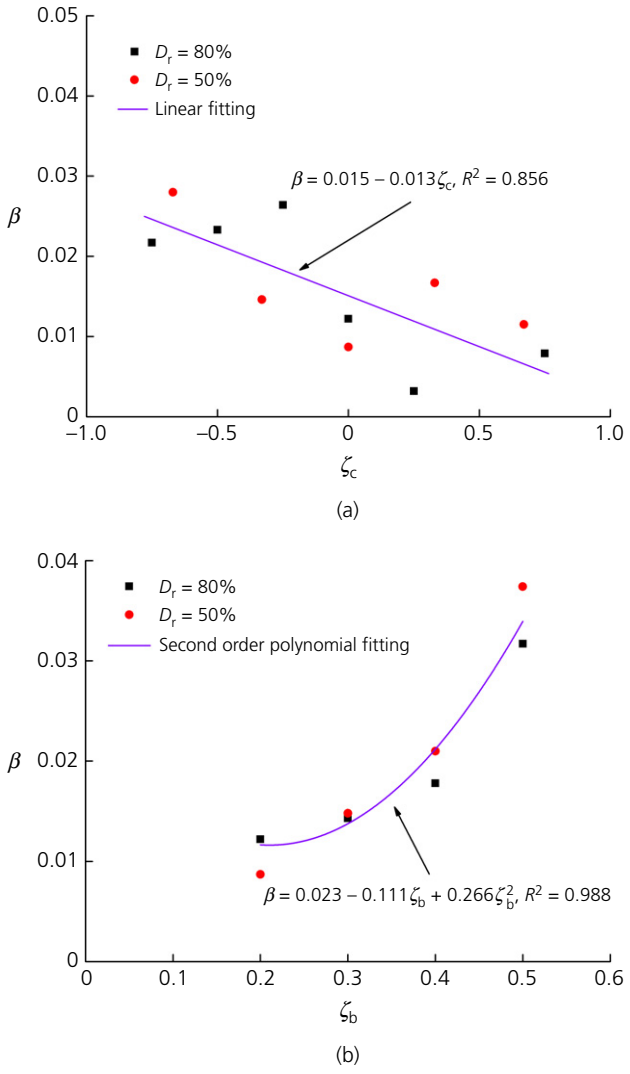

Figure 10. Cyclic dimensionless functions for changing in secant stiffness: (a) β–ζ_c and (b) β–ζ_b

From Figure 10(b), an increasing cyclic load magnitude leads to an increase in the relative secant stiffness accumulation rate, β. A second-order polynomial fit seems to capture the trend well, see Equation 8.

$$\beta = 0.023 - 0.111\zeta_b + 0.266\zeta_b^2 \quad (8)$$

From Figure 10, it is not possible to make a clear distinction between the results for $D_r = 80\%$ and $D_r = 50\%$. This indicates that β is somewhat independent of sand relative density.

4. Discussion and new design approach

The centrifuge testing results showed that the accumulated pile lateral displacement and evolution of secant stiffness depends on: (*a*) the number of cycles; (*b*) the magnitude and the directional characteristic of the load; (*c*) the relative density of the sand. Therefore, these two design parameters (i.e. accumulated lateral pile displacement and change in the foundation stiffness) can be predicted from the results of a monotonic test combined with a series of functions determined from results presented in the previous sections. Accordingly, a new design approach is developed in this section, an example of the application is presented and the performance is compared with the data from a field test on a laterally loaded monopile.

4.1 Functions to describe the evolution of accumulated lateral displacement

The results indicate that the displacement accumulation rate α is a function of load amplitude (ζ_b) and load directional characteristic (ζ_c). Assuming independence between these two parameters, α can be written as a superposition of two non-dimensional functions, each depending on only one of these two variables as described in Equation 9

$$\alpha(\zeta_c, \zeta_b) = T_c(\zeta_c)\, T_b(\zeta_b) \quad (9)$$

For one-way loading – that is, $\zeta_c = 0$ – T_c can be normalised as 1. Therefore, the non-dimensional function T_b can be found from a series of tests where ζ_b is changed while ζ_c is maintained at 0. These results from the centrifuge tests are depicted in Figure 11(a). It can be observed that the function $T_b(\zeta_b)$ is a constant function

$$\alpha(\zeta_c = 0,\ \zeta_b) = 1 \times T_b(\zeta_b) = 0.07335 \quad (10)$$

The function T_c, therefore, can be found by performing a series of tests with a constant ζ_b and then dividing the results

of α by the previously determined function $T_b(\zeta_b)$

11. $$T_c(\zeta_c) = \frac{\alpha}{T_b(\zeta_b)}$$

The results from Figure 7 indicate that for $\zeta_c > 0.2$ the value of $\alpha \approx 0.058$ for piles installed in either dense or medium dense sand layers. However, for $\zeta_c \leq 0.2$, the value of α as a function of the relative density of the sand layer can be described using two individual functions (as shown in Figure 11(b))

12. $$T_c(\zeta_c) = -1.707(\zeta_c + 0.31)^2 + 0.949 (D_r = 80\%)$$

13. $$T_c(\zeta_c) = -1.14(\zeta_c + 0.323)^2 + 1.263 (D_r = 50\%)$$

Therefore, provided that the value of $y_{max,S}$ is determined from a monotonic test and the relative density of the sand layer is known, the accumulated lateral displacement could be predicted for various combinations of amplitude and directional characteristic of loading for a certain number of cycles.

4.2 Functions to describe the evolution of secant stiffness

Similarly to the approach described for the prediction of the accumulated lateral displacement, the secant stiffness increment rate β can be written as a superposition of two non-dimensional functions as shown in Equation 14

14. $$\beta(\zeta_c, \zeta_b) = R_c(\zeta_c)\ R_b(\zeta_b)$$

For one-way loading, – that is $\zeta_c = 0$ – the value of R_c can be normalised as 1. Therefore, the relationship of non-dimensional functions R_b and ζ_b (as shown in Figure 12(a))

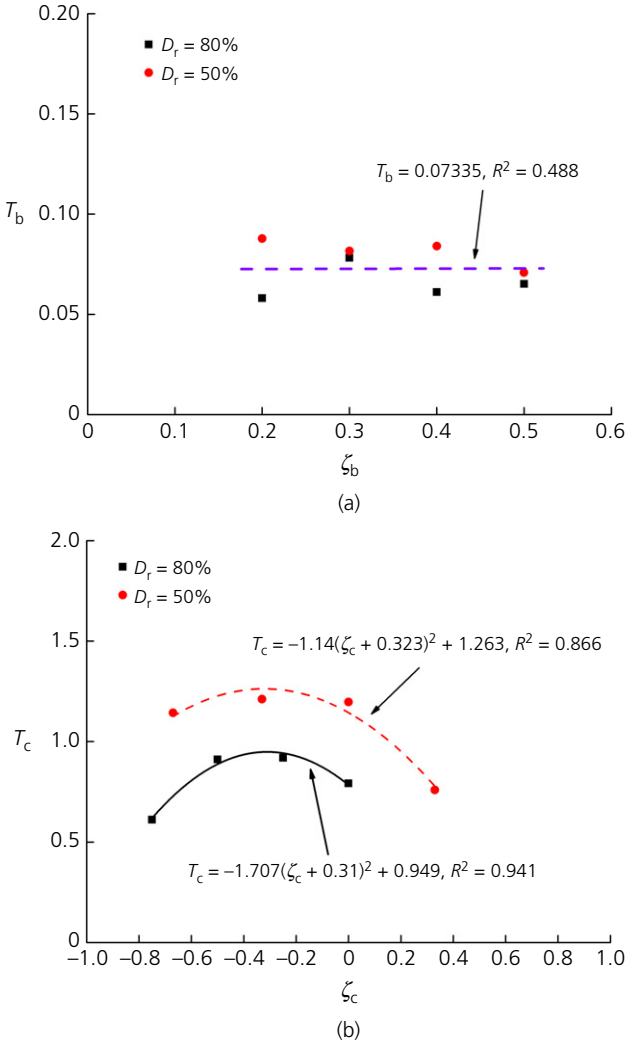

Figure 11. Dimensionless functions for accumulation of maximum lateral displacement: (a) T_b–ζ_b; (b) T_c–ζ_c

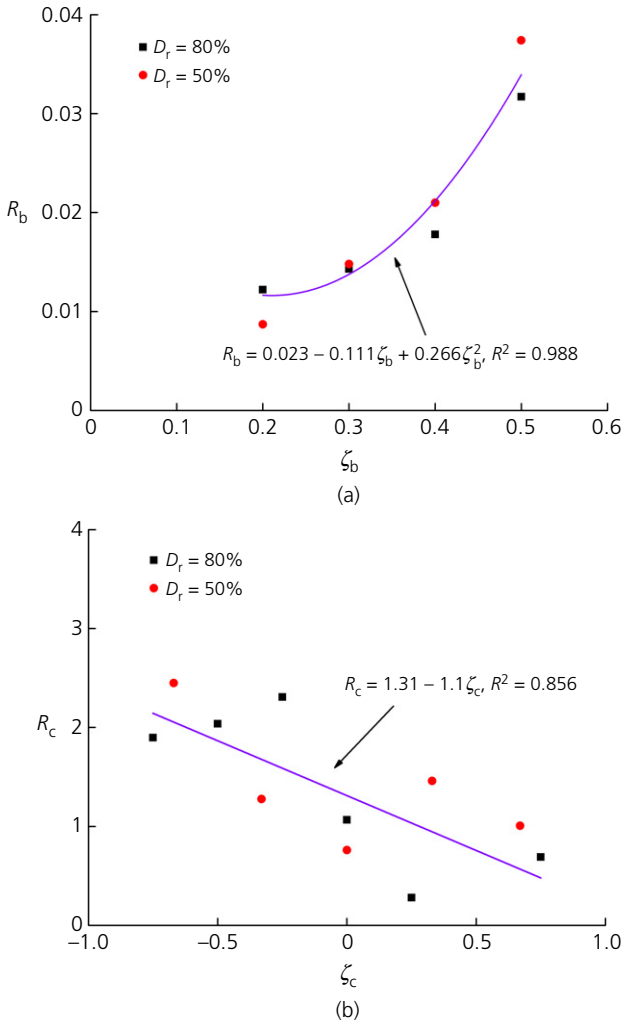

Figure 12. Dimensionless functions for evolution of secant stiffness: (a) R_b–ζ_b; (b) R_c–ζ_c

can be expressed by the following equation:

15. $$R_b(\zeta_b) = 0.023 - 0.111\zeta_b + 0.266\zeta_b^2$$

Figure 12(b) shows results for the cyclic load directional characteristic function R_c. The results seem to follow a linear relationship, see Equation 16

16. $$R_c(\zeta_c) = 1.31 - 1.1\zeta_c$$

All the R_c values are positive; this means that the cyclic secant stiffness K_N keeps increasing as a function of the number of cycles for all values of ζ_c. It should also be noticed that going from one-way to two-way loading leads to an increasing accumulation of stiffness. From Figure 12(a), an increase in the cyclic load magnitude leads to an increase in the secant stiffness accumulation rate β.

From Figure 12, it is not possible to make a clear distinction between the results for $D_r = 80\%$ and $D_r = 50\%$. This indicates that values of relative secant stiffness K_N / K_1 are somewhat independent of the sand relative density.

Therefore, provided that the value of K_1 is known, the secant stiffness of the pile could be predicted for various combinations of amplitude and directional characteristic of loading for a certain number of cycles. The next section describes an empirical procedure to determine the value of K_1.

4.3 Functions to describe the initial cyclic secant stiffness (K_1)

The cyclic secant stiffness at the first loading cycle $K_1(\zeta_c, \zeta_b)$ can be written as a superposition of two functions as shown in Equation 17

17. $$K_1(\zeta_c, \zeta_b) = K_c(\zeta_c)\, K_s(\zeta_b)$$

The value of K_1 can be found from the results of a set of monotonic test and cyclic tests with varying directional characteristics. The function $K_s(\zeta_b)$ can be established directly from one monotonic load–displacement curve, or from the monotonic loading phase of cyclic load test. The results are shown in Figure 13(a), and it can be seen that a linear fit captures well the variation of $K_s(\zeta_b)$

18. $$K_s(\zeta_b) = (72 - 56\zeta_b) \times 100\,\mathrm{kN/m}$$

$K_c(\zeta_c)$ is then evaluated from the cyclic tests, and the test results from this study are shown in Figure 13(b). It can be seen that a linear fit may also capture the trend of $K_c(\zeta_c)$

19. $$K_c(\zeta_c) = 0.057\zeta_c + 1.25$$

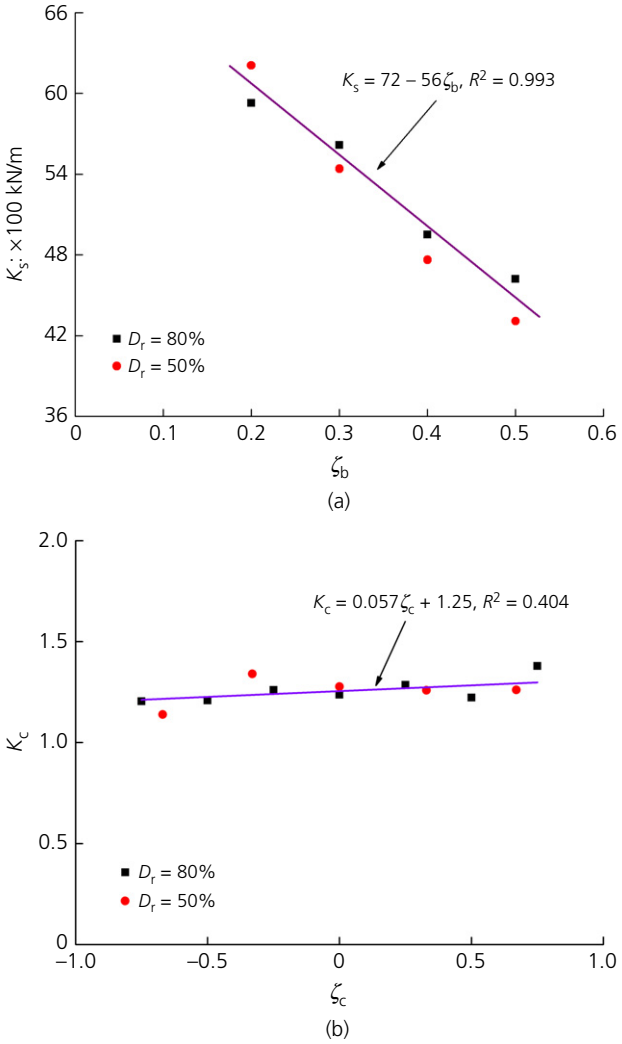

Figure 13. Functions for initial cyclic secant stiffness: (a) K_s–ζ_b; (b) K_c–ζ_c

Results shown in Figure 13 indicate that the secant stiffness functions of K_c and K_s are not sensitive to the sand relative density.

As all the non-dimensional functions ($T_c(\zeta_c)$, $T_b(\zeta_b)$, $R_c(\zeta_c)$, $R_b(\zeta_b)$, $K_c(\zeta_c)$) along with dimensional function $K_s(\zeta_b)$ are established, accumulation of maximum lateral displacements and change in secant stiffness depending on the number of cycles can be predicted by the proposed design procedure.

Although the design procedure was formulated based on tests with limited number of load cycles (maximum number of 153 cycles each test), it can be seen from the studies of Verdure *et al.* (2003), Leblanc *et al.* (2010), Li *et al.* (2010) and Klinkvort and Hededal (2013) that the overall pile displacement accumulation rate and change in secant stiffness at large load cycles (e.g. cycle number $N > 1000$) follow the same trend

captured within about 50 cycles. In agreement with the method proposed by Little and Briaud (1988) and Long and Vanneste (1994), the exponential behaviour of accumulated rotation plotted against cycle number appears as straight lines in double logarithmic axis for up to 10^5 cycles. Therefore, in the following, the pile behaviour under a large number of load cycles is predicted by extrapolating data measured in tests with a small number of load cycles.

4.4 Example

4.4.1 Demonstration of the proposed design procedure

A rigid pile with $D = 1.8$ m, embedded length of $L = 5D$ and load eccentricity of $e = 8D$ is considered in this example. The sand is assumed to be dry, with a friction angle of 35°. The goal is to predict the increase in secant stiffness and accumulated lateral displacement when the pile is subjected to 10^7 loading cycles with $\zeta_b = 0.3$ and $\zeta_c = -0.2$.

The dimensions of the pile in this example are selected to be similar to those of the prototype pile of this study, as the monotonic loading data, as the only required input for this model, are available (Figure 3). The results depicted in Figure 3 show that $\zeta_b = 0.3$ is equivalent to a maximum lateral load of $H_{max} = 0.3 \times 600$ kN $= 180$ kN and $H_{max} = 0.3 \times 440$ kN $= 132$ kN in dense and medium dense sand layers, respectively. The corresponding displacement $y_{max,S}$ is determined (from Figure 3) to be 0.02 m in dense and medium dense sand conditions.

Therefore, the accumulation rate of lateral displacement α can be calculated according to Equation 9 and Figure 11. The values of α are calculated to be 0.068 and 0.091 for the cases of dense and medium dense sand layers, respectively. Hence, using Equation 3, the accumulated lateral displacements after 10^7 cycles can be calculated as 2.99 and 4.34 times of $y_{max,S}$ (Equations 20 and 21), which are 0.06 m and 0.087 m in dense and medium dense sand, respectively.

20. $$\frac{y_{max,N}}{y_{max,S}} = N^{\alpha} = \left(10^7\right)^{0.068} \approx 2.99 \ (D_r = 80\%)$$

21. $$\frac{y_{max,N}}{y_{max,S}} = N^{\alpha} = \left(10^7\right)^{0.091} \approx 4.34 \ (D_r = 50\%)$$

By using $K_1(\zeta_c, \zeta_b)$, the accumulation rate of secant stiffness follows Equation 14. β is calculated to be 0.02 in both dense sand and medium dense sand, without difference. Then according to Equation 6

22. $$\frac{K_N}{K_1} = N^{\beta} = \left(10^7\right)^{0.02} = 1.38$$

This result indicates that the secant stiffness is estimated to increase by approximately 38% during the lifespan of the wind turbine.

4.4.2 Comparison with field test data and other prediction models

Li *et al.* (2015) conducted a field test on a rigid pile with a diameter of $D = 0.34$ m, and an embedded length of $L = 6.5D$. The pile was installed in a dense sand layer and loaded with an eccentricity $e = 1.2D$. More than 1000 one-way lateral load cycles were applied to the pile with $\zeta_b = 0.3$ and $\zeta_c = 0$. The monotonic load–displacement curve of this test indicates a $y_{max,S} = 0.0042$ m and, according to the loading features and using Equation 9 along with Figure 11, the accumulation rate of lateral displacement α can be calculated to be 0.07335. Therefore, the following equation can describe the pile accumulated displacement:

23. $$\frac{y_{max,N}}{y_{max,S}} = N^{\alpha} = (N)^{0.07335}$$

The pile rotation can be calculated by assuming the pile as a rigid body and the pile rotation point to be located at $0.7L$ beneath the sand surface (Chortis *et al.*, 2020; Haiderali *et al.*, 2014). Based on these assumptions, the relationship between the pile rotation at the sand surface and the cycle number can be established.

The comparison between predicted results by Little and Briaud (1988), LeBlanc *et al.* (2010), Klinkvort and Hededal (2013) and the present study and the field test data reported by Li *et al.* (2015) is shown in Figure 14. The model from this study provides a better prediction of the measured response.

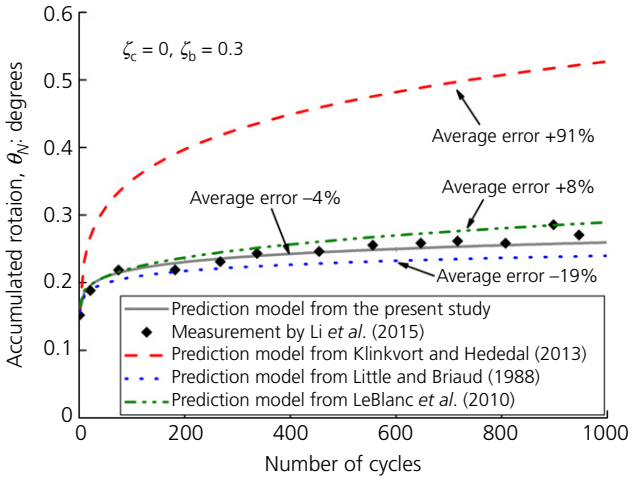

Figure 14. Comparison on the pile accumulated rotation between model predictions and field test data

The prediction model developed by Little and Briaud (1988) slightly underestimates the pile accumulated rotation (with an average error of −19%), while the prediction model developed by LeBlanc *et al.* (2010) slightly overestimates the pile accumulated rotation (with an average error of 8%). The model developed by Klinkvort and Hededal (2013) overestimates the pile accumulated rotation by up to 91%. As mentioned by Li *et al.* (2015), the variation in the prediction models partly results from soil variability and experimental measurement errors.

5. Conclusions

Centrifuge tests were carried out on an open-ended monopile with L/D ratio of 5 in dry sand with two relative densities of 50% and 80%, to evaluate cyclic load-induced accumulation of lateral displacement and evolution of secant stiffness. The focus was on two key parameters: cyclic load directional characteristic ratio (ζ_c) and cyclic magnitude ratio (ζ_b). Equations were formulated based on the test data for the prediction of accumulation of lateral displacement and change in secant stiffness of the pile. The following conclusions can be drawn.

(*a*) The most damaging cyclic load type is two-way loading, with $\zeta_c \approx -0.4$, regardless of the sand relative densities. When $\zeta_c \leq 0.2$, the pile exhibits a faster rate of generating accumulated maximum displacement in medium dense sand compared with that in dense sand. When $\zeta_c > 0.2$ (one-way cyclic loading), the pile maximum displacement accumulation rate was found not to be sensitive to the sand relative density. The pile displacement accumulation coefficient (α) was found not to be sensitive to the cyclic magnitude ratio (ζ_b).

(*b*) Cyclic loading results in an increase in the secant stiffness per cycle irrespective of the sand relative density. When the applied load was changed from one-way to two-way, an increasing rate of accumulation of secant stiffness was observed. An increase in the cyclic load magnitude ratio (ζ_b) led to an increase in the relative secant stiffness accumulation rate (β).

(*c*) The design procedure which can be applied for any combination of load amplitude, load directional characteristic and cycle number to predict pile lateral loading behaviour (originally established by Klinkvort and Hededal (2013)) was re-evaluated in this study. The related three sets of functions ($T_c(\zeta_c)$, $T_b(\zeta_b)$, $R_c(\zeta_c)$, $R_b(\zeta_b)$, $K_c(\zeta_c)$, $K_s(\zeta_b)$) were reformulated based on the centrifuge test results from this research. The accumulation of lateral displacement and the evolution of secant stiffness can therefore be predicted by a monotonic response together with the aforementioned functions. A power law function along with the parameters determined from this study was found to predict the pile response tested in the field by Li *et al.* (2015) with less than 5% average error.

The proposed prediction model is formulated based on certain kinds of pile and sand, and pile installation method. If prediction is going to be made on other types of piles, only the prediction procedure can be referred to. The non-dimensional and dimensional functions should be determined on the targeted pile and sand under the designed pile installation method. Moreover, it should be noted that the number of cycles applied to the piles tested in the centrifuge is several orders of magnitude smaller than those that monopiles experience in their lifetime.

Acknowledgements

The authors are grateful to Han J. de Visser, Kees van Beek, Ronald van Leeuwen, Leon Roessen, Bert Bakker and Karel Heller for their technical support to this study.

Funding information

This work is funded by the Section of Geo-Engineering, Delft University of Technology. The first author is supported by the China Scholarship Council (CSC).

REFERENCES

Abadie CN, Byrne BW and Houlsby GT (2018) Rigid pile response to cyclic lateral loading: laboratory tests. *Géotechnique* **69(10)**: 863–876, https://doi.org/10.1680/jgeot.16.P.325.

Allersma H (1994) The University of Delft geotechnical centrifuge. In *Proceedings of International Conference Centrifuge 94, Singapore* (Lee FH, Leung CF and Tan TS (eds)). Balkema, Rotterdam, the Netherlands, pp. 47–52.

Askarinejad A, Sitanggang APB and Schenkeveld F (2017) Effect of pore fluid on the behavior of laterally loaded offshore piles modelled in centrifuge. *Proceedings of 19th International Conference on Soil Mechanics and Geotechnical Engineering (ICSMGE 2017), Seoul, Korea*. CRC Press, pp. 897–900.

Chortis G, Askarinejad A, Prendergast L, Li Q and Gavin K (2020) Influence of scour depth and type on p–y curves for monopiles in sand under monotonic lateral loading in a geotechnical centrifuge. *Ocean Engineering* **197**, https://doi.org/10.1016/j.oceaneng.2019.106838.

De Jager RR, Maghsoudloo A, Askarinejad A and Molenkamp F (2017) Preliminary results of instrumented laboratory flow slides. In *Proceedings of the 1st International Conference on the Material Point Method (MPM 2017)* (Rohe A, Soga K, Teunissen H and Coelho BZ (eds)). Elsevier, Delft, the Netherlands, pp. 212–219.

Doherty P and Gavin K. (2011) Laterally loaded monopile design for offshore wind farms. *Proceedings of the Institution of Civil Engineers – Energy* **165(1)**: 7–17.

Fan S, Bienen B and Randolph MF (2019) Centrifuge study on effect of installation method on lateral response of monopiles in sand. *International Journal of Physical Modelling in Geotechnics* 1–13, https://doi.org/10.1680/jphmg.19.00013.

Garnier J, Gaudin C, Springman SM *et al.* (2007) Catalogue of scaling laws and similitude questions in geotechnical centrifuge modelling. *International Journal of Physical Modelling in Geotechnics* **7(3)**: 1–23, https://doi.org/10.1680/ijpmg.2007.070301.

Gerber TM and Rollins KM. (2008) Cyclic P–Y curves for a pile in cohesive soil. In *Geotechnical Earthquake Engineering and Soil Dynamics IV* (Zeng D, Manzari MT and Hiltunen DR (eds)). American Society of Civil Engineers, Reston, VA, USA, https://doi.org/10.1061/40975(318)139.

Gui M, Bolton M, Garnier J *et al.* (1998) Guidelines for cone penetration tests in sand. In *Centrifuge 98: Proceedings of the International Conference* (Kimura T, Kusakabe O and Takemura J (eds)). A. A. Balkema, Rotterdam, the Netherlands, pp. 155–160.

Haiderali AE, Lau BH, Haigh SK and Madabhushi SPG (2014) Lateral response of monopiles using centrifuge testing and finite element analysis. In *Physical Modelling in Geotechnics – Proceedings of the 8th International Conference on Physical Modelling in Geotechnics 2014, ICPMG 2014*, vol. 2, pp. 743–749.

Klinkvort RT and Hededal O. (2013) Lateral response of monopile supporting an offshore wind turbine. *Proceedings of the Institution of Civil Engineers – Geotechnical Engineering* **166(2)**: 147–158, https://doi.org/10.1680/geng.12.00033.

Klinkvort RT, Hededal O and Svensson M (2011) Laterally cyclic loading of monopile in dense sand. In *Proceedings of the 15th European Conference on Soil Mechanics and Geotechnical Engineering* (Anagnostopoulos A, Pachakis M and Tsatsanifos C (eds)). IOS Press, Amsterdam, the Netherlands, pp. 203–208.

Leblanc C, Houlsby G and Byrne B. (2010) Response of stiff piles in sand to long-term cyclic lateral loading. *Géotechnique* **60(2)**: 79–90, https://doi.org/10.1680/geot.7.00196.

Li Z, Haigh S and Bolton M (2010) Centrifuge modelling of mono-pile under cyclic lateral loads. In *Proceedings of the 7th International Conference on Physical Modelling in Geotechnics, Zurich*, vol. 2, 965–970.

Li W, Igoe D and Gavin K. (2015) Field tests to investigate the cyclic response of monopiles in sand. *Proceedings of the Institution of Civil Engineers – Geotechnical Engineering* **168(5)**: 407–421, https://doi.org/10.1680/jgeen.14.00104.

Li Q, Prendergast L, Askarinejad A, Chortis G and Gavin K. (2020) Centrifuge modeling of the impact of local and global scour erosion on the monotonic lateral response of a monopile in sand. *Geotechnical Testing Journal* **43(5)**: 1084–1100.

Little RL and Briaud JL (1988) *Full Scale Cyclic Lateral Load Tests on Six Single Piles in Sand*. Department of Civil EngineeringTexas A & M University, College Station, TX, USA.

Long J and Vanneste G (1994) Effects of cyclic lateral loads on piles in sand. *J. Geotech. Engng* **120(1)**: 225–244.

Maghsoudloo A, Galavi V, Hicks MA and Askarinejad A (2017) Finite element simulation of static liquefaction of submerged sand slopes using a multilaminate model. *ICSMGE 2017 – 19th International Conference on Soil Mechanics and Geotechnical Engineering, Seoul, Korea*. International Society of Soil Mechanics and Geotechnical Engineering, London, UK, vol. 2, pp. 801–804.

Maghsoudloo A, Askarinejad A, De Jager R, Molenkamp F and Hicks M (2018) Experimental investigation of pore pressure and acceleration development in static liquefaction induced failures in submerged slopes. In *Proceedings of the 9th International Conference of Physical Modelling in Geotechnics* (McNamara A, Divall S, Goodey R *et al.* (eds)). CRC Press, London, UK, vol. 2, pp. 987–992.

Møller IF and Christiansen T (2011) *Laterally Loaded Monopile in Dry and Saturated Sand – Static and Cyclic Loading: Experimental and Numerical Studies*. Masters project, Aalborg University.

Nicolai G, Ibsen LB, O'loughlin C and White D. (2017) Quantifying the increase in lateral capacity of monopiles in sand due to cyclic loading. *Géotechnique Letters* **7(3)**: 245–252, https://doi.org/10.1680/jgele.16.00187.

Nunez I, Hoadley P, Randolph M and Hulett J (1988) Driving and tension loading of piles in sand on a centrifuge. *Proceedings of Centrifuge 88* (Corte JF (ed.)). A. A. Balkema, Rotterdam, the Netherlands, pp. 353–362.

Peralta P (2010) *Investigations on the Behavior of Large Diameter Piles under Long-term Lateral Cyclic Loading in Cohesionless Soil*. Institut für Geotechnik, Hannover, Germany.

Remaud D (1999) *Pieux Sous Charges Latérales: Étude Expérimentale de l'Effet de Groupe*. These de Doctorat, University of Nantes, Nantes, France (in French).

Roesen HR, Ibsen LB and Andersen LV (2012) Small-scale testing rig for long-term cyclically loaded monopiles in cohesionless soil. *The Nordic Geotechnical Meeting, Dansk Geoteknisk Forening*, pp. 435–442.

Truong P, Lehane B, Zania V and Klinkvort RT (2018) Empirical approach based on centrifuge testing for cyclic deformations of laterally loaded piles in sand. *Géotechnique* **69(2)**: 133–145, https://doi.org/10.1680/jgeot.17.P.203.

Verdure L, Garnier J and Levacher D. (2003) Lateral cyclic loading of single piles in sand. *International Journal of Physical Modelling in Geotechnics* **3(3)**: 17–28.

Wu X, Hu Y, Li Y *et al.* (2019) Foundations of offshore wind turbines: a review. *Renewable and Sustainable Energy Reviews* **104**: 379–393.

Yang QJ, Gao YF, Kong DQ and Zhu B. (2019) Centrifuge modelling of lateral loading behaviour of a 'semi-rigid' mono-pile in soft clay. *Marine Georesources & Geotechnology* **37**, **10**: 1205–1216.

Yoo MT, Choi JI, Han JT and Kim MM. (2013) Dynamic P-Y curves for dry sand from centrifuge tests. *Journal of Earthquake Engineering* **17(7)**: 1082–1102.

Zhang W and Askarinejad A (2019a) Behaviour of buried pipes in unstable sandy slopes. *Landslides* **16(2)**: 283–293.

Zhang W and Askarinejad A (2019b) Centrifuge modelling of submarine landslides due to static liquefaction. *Landslides* **16(10)**: 1007.

How can you contribute?

To discuss this paper, please email up to 500 words to the editor at journals@ice.org.uk. Your contribution will be forwarded to the author(s) for a reply and, if considered appropriate by the editorial board, it will be published as discussion in a future issue of the journal.

Proceedings journals rely entirely on contributions from the civil engineering profession (and allied disciplines). Information about how to submit your paper online is available at www.icevirtuallibrary.com/page/authors, where you will also find detailed author guidelines.